Ceramics International 44 (2018) 19397–19401

Contents lists available at ScienceDirect

Ceramics International

journal homepage: www.elsevier.com/locate/ceramint

Sol-gel synthesis of triclinic CoV_2O_6 polycrystals

Driele von Dreifus[a,b,*], Rodrigo Pereira[c], Ariano D. Rodrigues[a], Ernesto C. Pereira[b], Adilson J.A. de Oliveira[a]

[a] Departamento de Física, Universidade Federal de São Carlos (UFSCar), São Carlos, SP, Brazil
[b] Departamento de Química, Universidade Federal de São Carlos (UFSCar), São Carlos, SP, Brazil
[c] Instituto Federal de Educação, Ciência e Tecnologia de Mato Grosso (IFMT), São Vicente, MT, Brazil

ARTICLE INFO

Keywords:
γ-CoV_2O_6 polycrystals
γ-CoV_2O_6 synthesis
γ-CoV_2O_6 crystalline structure
γ-CoV_2O_6 vibrational modes
γ-CoV_2O_6 magnetic properties

ABSTRACT

In this paper, a new chemical route synthesis for γ-CoV_2O_6 is proposed. Based on the CoO-V_2O_5 phase diagram a study of temperature and calcination times for pure γ-CoV_2O_6 obtainment is described. X-ray diffraction and Raman spectroscopy experiments revealed the triclinic crystals structure belonging to P-1 spatial group. FEG-SEM images showed that the resulting grains present elongated shape. Rietveld analysis revealed a crystalline anisotropy with preferential crystallographic orientation in the [2 0 − 1] and [1 3 0] planes. The calculated mean crystallite size evidences that the crystallite dimensions are significantly different in the parallel and perpendicular directions. The magnetic properties measurements evidenced an antiferromagnetic transition at 7 K and a detailed view of the magnetization isotherms confirmed a noticeable step-like behavior below T_N, characteristic of field-induced transitions.

1. Introduction

Transition metal vanadium oxides have attracted enormous attention in contemporary solid state chemistry and physics due to their rich physical properties. Cobalt-based vanadates are representative vanadium oxides that due to their electrochemical, catalytic, and magnetic properties many scientists devoted efforts to synthesize [1–4].

CoV_2O_6 can crystallize in two crystalline structures: monoclinic (α–CoV_2O_6) and triclinic (γ–CoV_2O_6) [5]. Reports describing syntheses and physical properties of CoV_2O_6 with monoclinic structure [6–9] are much more frequently found than with triclinic symmetry [10,11]. Taking into account the CoO-V_2O_5 phase diagram, one can verify that at high temperatures (~ 700 °C) and with adequate stoichiometry, there is a narrow range in which it is possible to achieve the monoclinic phase without the presence of other oxides [5]. Although the decrease in the calcination temperature (< 600 °C) favors the formation of the triclinic phase, this region in the diagram is surrounded by the possibility of V_2O_5, α–CoV_2O_6 and $Co_2V_2O_7$ coexistence. Thus the adjustment of calcination and synthesis conditions to obtain CoV_2O_6 in both crystalline structures is a challenging task. Literature reports γ–CoV_2O_6 single crystals growth [2,3] and also γ–CoV_2O_6 polycrystals [10] using solid-state reaction method and a citrate decomposition method [12]. Despite the good quality of the samples produced by these methods, the employed thermal treatments require periods of 12 up to 45 h.

In this work, we propose an alternative chemical route for γ-CoV_2O_6 polycrystals synthesis based on the Pechini Method, a sol-gel route. The method's advantages include high homogeneity, reproducibility and short thermal treatment times at relatively low temperatures, without the need of laborious chemical processes [13]. The microstructural characterization and its correlation with the magnetic properties are also discussed while in the triclinic phase, CoV_2O_6 is composed by quasi-one-dimensional chains of edge-sharing CoO_6 octahedra in which Co atoms interact ferromagnetically intrachain and antiferromagnetically interchain, being separated by nonmagnetic V^{5+} ions in oxides blocks [2]. In addition, this system presents not only a temperature-dependent magnetic phase transition but also field-induced phase transitions that generate a step-like behavior in the magnetization curve by which this material is so recognized [3,10,12].

2. Experimental

γ-CoV_2O_6 polycrystals were synthesized by Pechini Method [14]. A precursor solution was prepared using anhydrous citric acid (AC-Synth) added to ethyleneglycol (EG- Mallinckrodt). The solution was kept under stirring at 70 °C during the entire process. NH_4VO_3 (M-Synth) was added to the solution respecting the 1:16:64 (M:CA:EG) molar proportion. Afterwards, $CoSO_4{\cdot}7H_2O$ (Synth), with 50 mol% of concentration, was slowly added to the mixture. The final solution was

* Correspondence at: Departamento de Física, Universidade Federal de São Carlos (UFSCar), São Carlos, SP, Brazil
E-mail address: dreifus@df.ufscar.br (D. von Dreifus).

https://doi.org/10.1016/j.ceramint.2018.07.171
Received 16 May 2018; Received in revised form 18 July 2018; Accepted 18 July 2018
Available online 19 July 2018

then polymerized at 110 °C and thermally treated at 300 °C during 2 h.

The powder obtained were divided into eight mass equal parts (S1, S2, S3, S4, S5, S6, S7 and S8) that were subjected to a systematic study of calcination time and calcination temperature for obtaining γ-CoV_2O_6 monophasic samples. In this study, one group composed by S1, S2, S3 and S4 was calcined at 500 °C, during 2 h (hours), 4 h, 6 h or 10 h, respectively. The other group, composed by S5, S6, S7 and S8 was calcined at 550 °C also during 2 h, 4 h, 6 h or 10 h, respectively. The calcination process was performed under air atmosphere and burning temperatures were chosen based on the CoO-V_2O_5 phase diagram [5] which presents the possibility of triclinic CoV_2O_6 samples obtainment, with or without the presence of V_2O_5 or other vanadates, since adequate synthesis stoichiometry and temperature range are used. For thermal treatment the heating ramp rate was 20 °C/min and the cooling rate was 5 °C/min.

The composition of all samples was verified by X-ray diffraction (XRD) measurements performed using CuKα radiation with a wavelength of 1.54 Å using a 2θ scan from 10° to 110° with 0.02° of increment. Field Emission Gun Scanning Electron Microscopy (FEG-SEM) was used for morphology and microstructure exploration. As grown, the powder samples were dispersed in acetone and gently sonicated. The dispersions were pipetted on silicon substrates. The electric contact between sample the holder and silicon substrate was made using silver paste. The same arrangement was used for EDX mapping.

In addition to XRD measurements, the sample that presented only the triclinic CoV_2O_6 was also characterized by Raman Spectroscopy. XRD data was analyzed by Rietveld refinement method [15,16] using GSA/EXPGUI [17,18] software. Raman spectra were recorded by a triple grating spectrometer, using a laser with a wavelength of 488 nm (~ 2.5 eV) as the excitation source in backscattering geometry.

As γ-CoV_2O_6 is very known due to its step-like magnetization curves behavior, its magnetic properties were investigated using a SQUID-VSM magnetometer (MPMS®3-Quantum Design). Magnetic susceptibility (χ) as a function of applied magnetic field (H), up to 70k Oe, and magnetic susceptibility (χ) as a function of temperature (T, 3–100 K) measurements, using zero field cooled (ZFC) and field cooled (FC) protocols were performed.

3. Results and discussion

3.1. Structural and morphological properties

As described in the Experimental section the powder obtained after the first thermal treatment were divided into eight equal mass parts, called S1, S2, S3, S4, S5, S6, S7 and S8 samples. Fig. 1 shows XRD data for this set of samples. One can observe that, except in S8, the presence of γ-CoV_2O_6 is accompanied by CoV_3O_8 phase indicated by asterisks in XRD graphs. This data analysis shows that in addition to long calcination times the obtainment of pure γ-CoV_2O_6 phase requires a thermal treatment at 550 °C, while the treatments carried out at 500 °C produced samples with the presence of CoV_3O_8 phase, despite the calcination during 10 h.

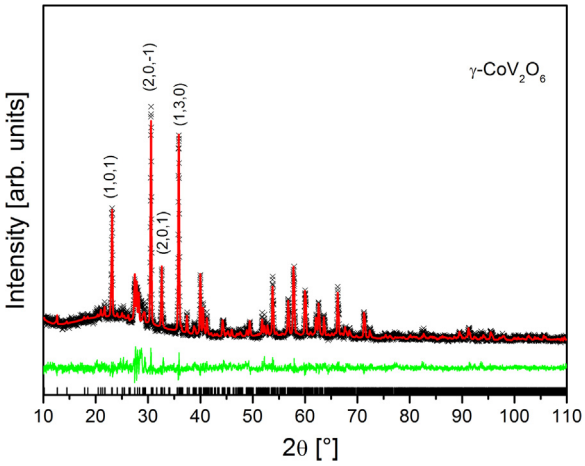

Fig. 2. Concordance between XRD data and the fit obtained by Rietveld refinement for a γ-CoV_2O_6 sample (S8). The black curve represents the diffraction profile of the sample, the red curve shows the fit obtained and the green curve is the difference between calculated and measured profiles. Black bars correspond to the Bragg peaks of the γ-CoV_2O_6 pattern (JCPS ICSD # 040849). (For interpretation of the references to color in this figure legend, the reader is referred to the web version of this article.)

S8 XRD data was analyzed by Rietveld method in order to confirm the absence of spurious phases. The results exclusively revealed the presence of triclinic CoV_2O_6 phase (Fig. 2), belonging to the P-1 spatial group. The lattice parameters obtained for this phase were a = 7.171(2) Å, b = 8.899(7) Å, c = 4.812(7) Å and α = 89.99(3)°, β = 93.72(7)°, γ = 101.86(5)° which are in good agreement with the pattern used for comparison (JCPS ICSD # 040849). Rietveld analysis showed that the samples exhibit crystalline anisotropy with preferential crystallographic orientation in the [2 0 − 1] and [1 3 0] directions highlighted in Fig. 2. The mean crystallite size (D) was calculated in two directions, parallel ($D_{\parallel}$ = 446 nm) and perpendicular ($D^{\perp}$ = 857 nm). Rietveld quality factors (χ^2 = 2.27 and Rwp = 0.150) showed conformity

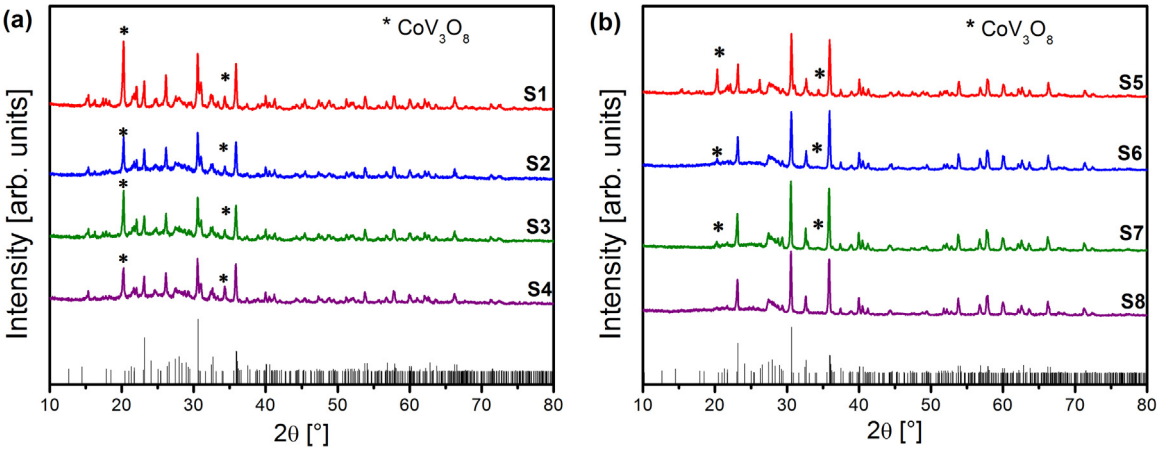

Fig. 1. Intensity (I) versus 2θ data of XRD measurements of samples calcined at (a) 500 °C during 2 h (S1), 4 h (S2), 6 h (S3) and 10 h (S4) and (b) 550 °C during 2 h (S5), 4 h (S6), 6 h (S7) and 10 h (S8). The black bars refer to the diffraction pattern of γ-CoV_2O_6 (JCPS ICSD # 040849) that is present in all samples and the asterisk (*) marks the position of the peaks related to the spurious phase CoV_3O_8. As can be seen in (b), only the samples calcined at 550 °C during 10 h (S8) do not exhibit undesirable phases.

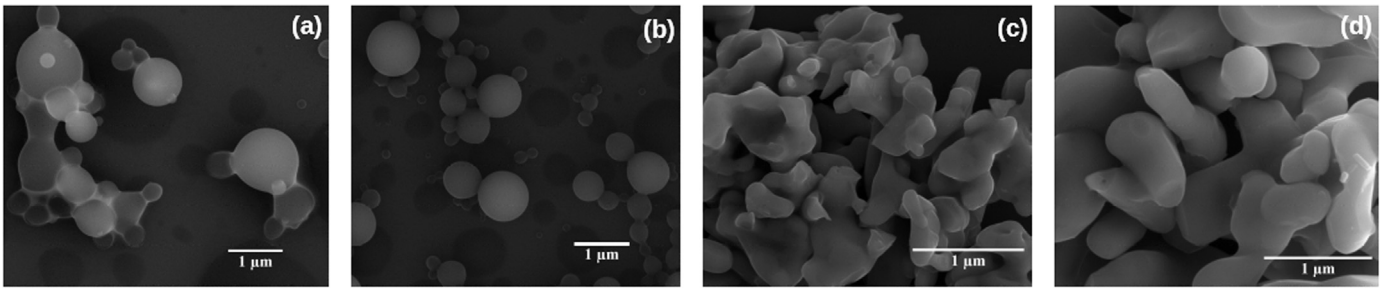

Fig. 3. FEG-SEM images show particle growth process evolution for samples calcined at 550 °C for (a) 2 h (S5), (b) 4 h (S6), (c) 6 h (S7) and (d) for 10 h (S8). The magnification images are 50,000x in a, b,c and 100,000x in d.

between experimental data and the fit curve. This can be confirmed by the good data fit and the small difference among measured and calculated profiles shown in Fig. 2.

Although a long calcination time is necessary for pure γ-CoV_2O_6 formation, FEG-SEM images demonstrate that the longer the calcination time, the particles, which were initially rounded, gain necks and become elongated, a characteristic of a sintering process. In Fig. 3a-d the evolution of this process is presented, showing particles with lengths around 1 µm. Although samples calcined for less than 10 h presented smaller particles and more regular shapes, XRD data of these samples showed the presence of secondary phases instead of γ-CoV_2O_6.

In the EDX (Energy Dispersive X-Ray spectroscopy) spectrum of S8 (Fig. 4) only peaks associated to C, O, Co, Si and V atoms are present. In this case, C and Si atoms are part of the sample holder used in the analysis.

A mapping obtained by the same technique in the same region in S8 (Fig. 5) demonstrated that the ratio between V and Co atoms over the whole survey area present no deviation from 65%:34%, V%:Co% ratio, which is the expected for γ-CoV2O6 stoichiometry. A possible presence of undesirable phases such as CoV_3O_8, for example, would result in a strong increase of ratio V%:Co% to around 75%:25%, whose variation would be identified as a contrast in the map. Additionally, the homogeneity of EDX signals indicates the absence of possible segregation of elements or the formation of other types of compounds.

3.2. γ-CoV_2O_6 vibrational modes

The Raman spectrum of the pure γ-CoV_2O_6 sample is presented in the range of the vibrational modes of vanadium-oxygen bonds with its respective fit, considering five spectral elements (Fig. 6). The peak assigned as (*) with wavenumber (full width at half maximum) 775 cm^{-1} (25 cm^{-1}) is related to V-O-V symmetric stretching. Peaks marked as (◆) with parameters 851 cm^{-1} (18 cm^{-1}) and 913 cm^{-1} (21 cm^{-1})

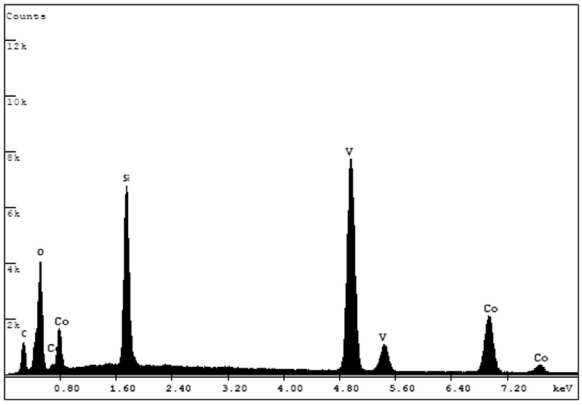

Fig. 4. EDX spectrum for the γ-CoV2O6 sample indicating the presence of Co, O and V atoms. Carbon (C) and silicon (Si) present in the spectrum are part of the sample holder used in the analysis.

are associated to V-O antisymmetric vibrations, while the peak identified as (°) with 946 cm^{-1} (15 cm^{-1}) is related to V-O symmetric vibrations [19,20]. In vanadates with monoclinic structures (C2/m spatial group) only these mentioned peaks are present for this spectral range [19–21]. However, in our sample, and additional peak at 829 cm^{-1} (13 cm^{-1}), marked as (+) occurs. This peak can be attributed to a splitting due to the lower symmetry of the triclinic structure [22]. The full widths at half maximums are similar to those found in other types of vanadates in which thermal treatments were applied to induce the maximum crystallization [23] confirming the high level of crystalline ordering in the formed particles.

3.3. Magnetic properties

The magnetic susceptibility (χ) measured for a field of 100 Oe (Fig. 7a) increases as the temperature decreases. At 7 K a sharp peak, associated with Néel Temperature (T_N) of the system [3] is observed for fields below 10k Oe. For very low temperatures ($T < 4$ K, $H = 100$ Oe) the system presents little irreversibility, considering that the values of magnetization obtained in FC are higher than those obtained in ZFC (Fig. 7a). For $H = 10$ kOe (Fig. 7b) the applied field is sufficient to align all the magnetic moments and this irreversibility is not observed between the ZFC and FC curves. For this field the antiferromagnetic transition is also suppressed.

The M(H) isotherms obtained above T_N behave as in soft ferromagnets in which moments are easily reversed by the magnetic field as observed in Fig. 8.

Although below T_N the magnetization isotherms increase rapidly with the rise of the applied magnetic field (Fig. 9a), the field intensity is not strong enough to complete the magnetization saturation. For comparison, as Lenertz et al. [24] observed a M_S of 2.8 μ_B/Co for $H = 70$ k Oe for γ-CoV_2O_6 single crystals and Kimber et al. [12] reported a M_S of 2.9 μ_B/Co for $H = 90$k Oe for polycrystalline samples, the maximum value of magnetization obtained at 70 kOe ($M_S = 3.2$ μ_B/Co) was considered as an estimate of magnetization saturation for our system. The difference between the M_S value obtained by us and the value due solely to the magnetic moment of the cobalt atom spin is reported in the literature as being associated with an orbital contribution from local distortions in the CoO_6 octahedra [8,25]. At 1.8 K the system exhibit a remnant magnetization (M_R) of 3.2×10^{-1} emu/g and a coercive field (H_C) of 100 Oe. In contrast, at 7 K the values of M_R and H_C decline to 9.3×10^{-2} emu/g and 80 Oe, respectively.

A detailed view of the low-field region at 1.8 K (Fig. 9b) exposes the step-like magnetization, a remarkable characteristic of this system [3,4,12,26]. The jump observed at about 6k Oe, indicated by a red asterisk in Fig. 9b, is related to the plateau characteristic of the magnetization curve of this material that occurs at around 1/3 of the M_S. In general, this plateau is more evident in monocrystalline γ-CoV_2O_6 samples [3] and even clearer in the monoclinic phase [27]. The system presents a considerable hysteresis 1/3 M_S at 1.8 K (Fig. 9b) and as well as the irreversibility observed in the temperature-dependent susceptibility curves can be related to ferromagnetic interactions that exist

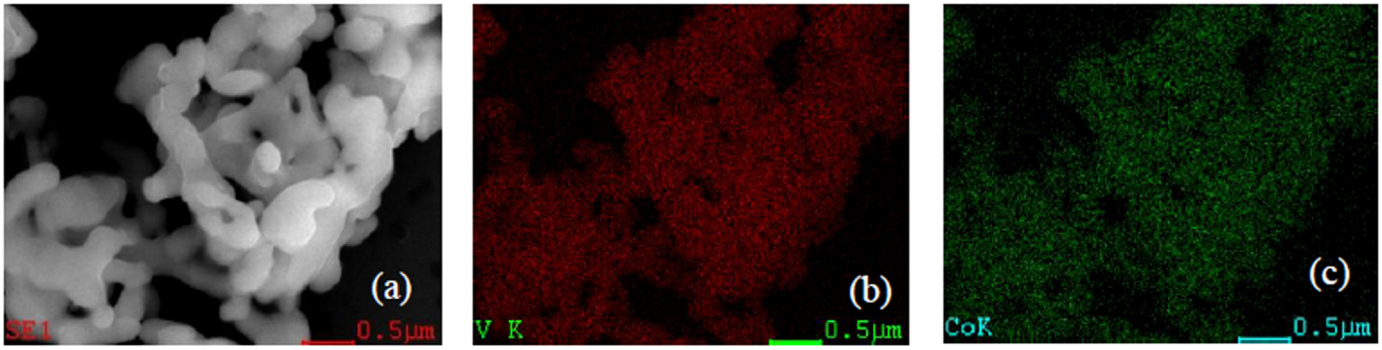

Fig. 5. Mapping obtained by EDX technique for a γ-CoV_2O_6 sample (S8). In (a) the analyzed region, in (b) the distribution of vanadium atoms and in (c) the distribution of cobalt atoms. The mapping showed a homogeneous distribution of V and Co atoms in the region analyzed. In addition, it was confirmed that the ratio between V and Co atoms is 65%: 34%, respectively.

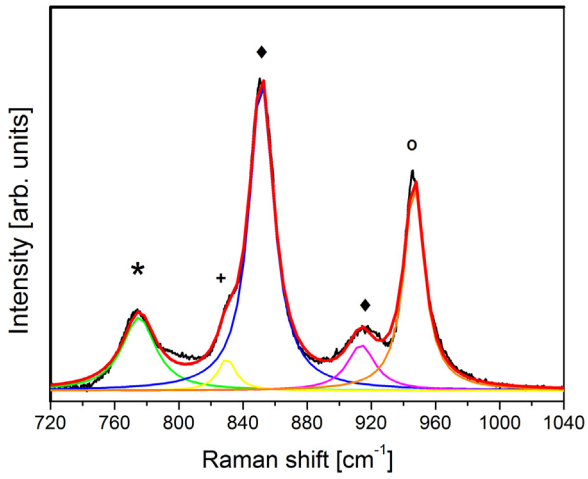

Fig. 6. Raman spectrum of γ-CoV_2O_6 at room temperature in the range of vanadium-oxygen vibrational modes and the respective fit, using five spectral elements, for 488 nm laser source excitation.

between the cobalt intrachain atoms in the material, although the cobalt inter-chain interaction in this material has antiferromagnetic nature [4,24]. According to Lenertz et al. [10] the presence of two types of interactions in the chain has its origin in the canting angle that exists between two adjacent Co-Co bonds which leads to a chain distortion and consequently an anisotropic behavior.

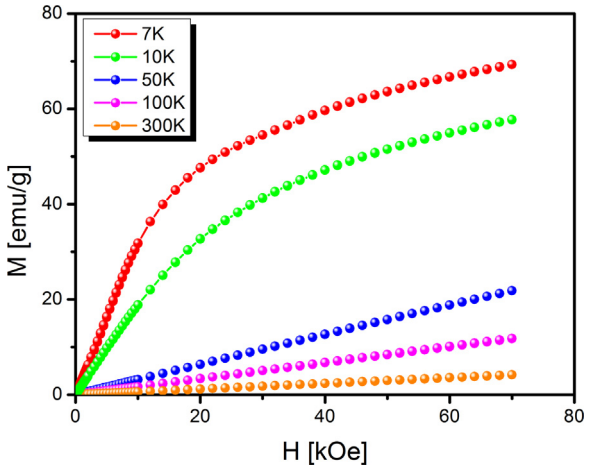

Fig. 8. Magnetization (M) as a function of magnetic applied field (H) curves for γ-CoV_2O_6 sample at 7 K, 10 K, 50 K, 100 K and 300 K.

4. Conclusions

Ideal conditions for monophasic γ-CoV_2O_6 polycrystalline synthesis by Pechini method were achieved. X-ray diffraction data revealed the triclinic symmetry of CoV_2O_6 and discharged the presence of spurious phases in sample S8. EDX mapping confirmed the stoichiometry between cobalt and vanadium atoms and the absence of other elements in the samples which could alter principally the magnetic properties. The

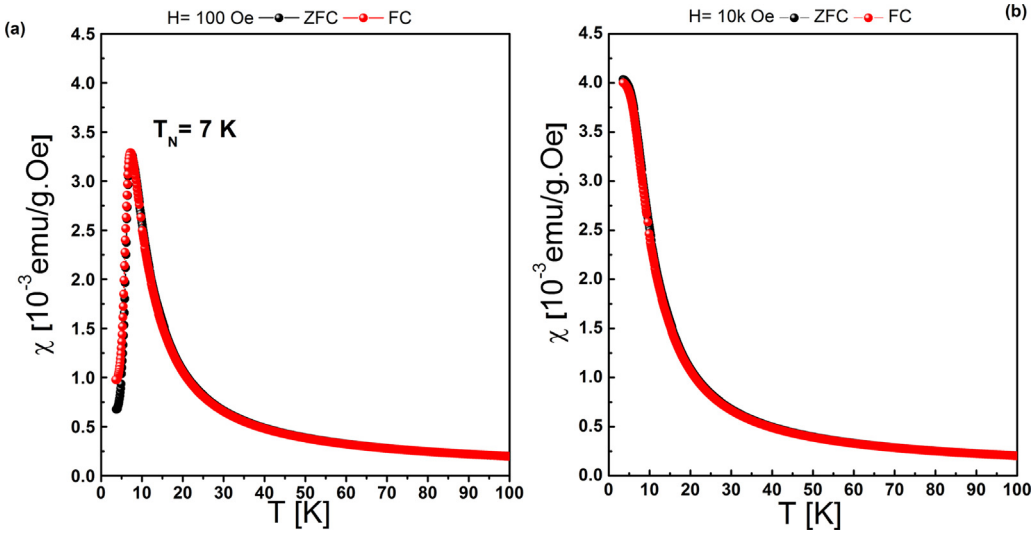

Fig. 7. Magnetic susceptibility (χ) curves as a function of temperature (T). Black circles indicate ZFC curves and red circles the FC curves at constant fields of (a) 100 Oe and (b) 10 k Oe. The Néel temperature for γ-CoV_2O_6 is indicated by a maximum in the curve as being T_N = 7 K. For H = 10k Oe the peak related to the antiferromagnetic transition is suppressed. (For interpretation of the references to color in this figure legend, the reader is referred to the web version of this article.)

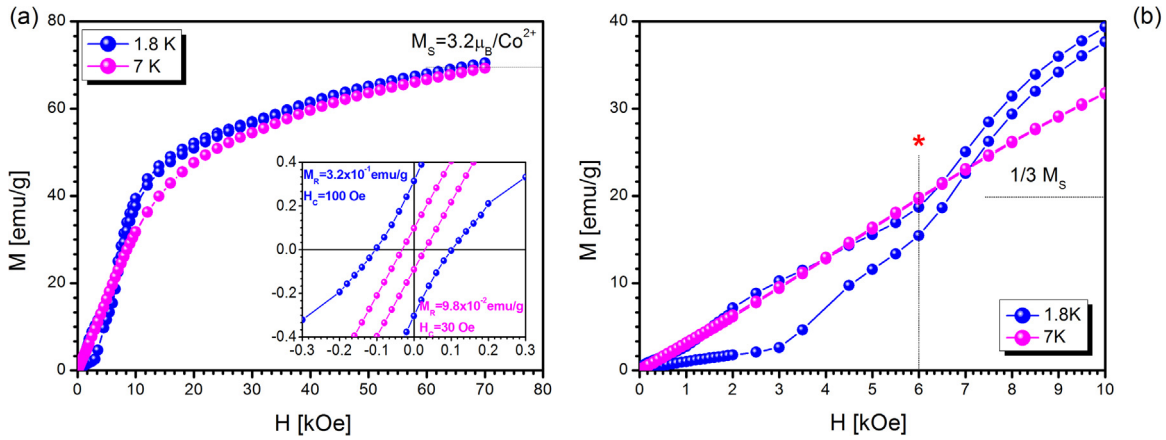

Fig. 9. (a) Magnetization curve (M) as a function of applied field (H) for γ-CoV_2O_6 sample S8 at 1.8 K and 7 K. The inset highlights the values of M_R and H_C for both isotherms. M_S is estimated as being 3.2 μ_B/Co for these temperatures. In (b) the low-field region of M vs H highlights the step-like behavior of γ-CoV_2O_6. The jump in magnetization curve, associated with 1/3 of M_S is indicated by *.

Raman spectrum obtained for the monophasic sample reveals the vibrational modes associated to the triclinic CoV_2O_6. Magnetization isotherms confirmed the step-like behavior as expected for γ-CoV_2O_6, although the polycrystalline nature of the samples overshadows a clear observation of the plateaus at 1/3 M_S in the magnetization curves below Néel temperature which was determined as being 7 K. The confirmation of sample purity by means of X-ray diffraction, EDX mapping and Raman spectroscopy techniques and the observation of the expected magnetic properties for this phase validate the proposed synthesis method that have as main advantages the homogeneity of samples and the short-term thermal treatment at low temperatures without the need for laborious chemical processes.

Acknowledgments

The authors thank FAPESP (09/54082-2 and 13/07296-2) and CNPq (500327/2014-9) for the financial support and the laboratory technician Rorivaldo de Camargo (UFSCar) who assisted in the EDX experiment.

References

[1] T. Mousavand, T. Naka, K. Sato, S. Ohara, M. Umetsu, S. Takami, T. Nakane, A. Matsushita, T. Adschiri, Crystal size and magnetic field effects in Co3O4 antiferromagnetic nanocrystals, Phys. Rev. B 79 (2009) 1–5, https://doi.org/10.1103/PhysRevB.79.144411.

[2] Y. Drees, S. Agrestini, O. Zaharko, A.C. Komarek, Floating zone single crystal growth of γ-CoV_2 O_6 with substantially enhanced crystal size and quality, Cryst. Growth Des. 15 (2015) 1168–1172, https://doi.org/10.1021/cg5015303.

[3] Z. He, M. Itoh, Single crystal flux growth of the Ising spin-chain system gama-CoV2O6, J. Cryst. Growth 388 (2014) 103–106, https://doi.org/10.1016/j.jcrysgro.2013.11.078.

[4] M. Lenertz, Propriétés structurales et magnétiques de cobaltites de type CoV2O6 à structure unidimensionnelle avec un intérêt potentiel pour la spintronique, Université De Strasbourg, Strasbourg, France, 2013.

[5] C. Brisi, Ann. Chim. 47 (1957) 815.

[6] Z. He, J.I. Yamaura, Y. Ueda, W. Cheng, CoV2O6 single crystals grown in a closed crucible: unusual magnetic behaviors with large anisotropy and 1/3 magnetization plateau, J. Am. Chem. Soc. 131 (2009) 7554–7555, https://doi.org/10.1021/ja902623b.

[7] H. Shu, Z.W. Ouyang, Y.C. Sun, M.Y. Ruan, J.J. Li, X.Y. Yue, Z.X. Wang, Z.C. Xia, G.H. Rao, Size-dependent magnetism in nanocrystals of spin-chain α-CoV2O6, J. Magn. Magn. Mater. 407 (2016) 129–134, https://doi.org/10.1016/j.jmmm.2016.01.063.

[8] K. Singh, A. Maignan, D. Pelloquin, O. Perez, C. Simon, Magnetodielectric coupling and magnetization plateaus in α-CoV2O6 crystals, J. Mater. Chem. 22 (2012) 6436–6440, https://doi.org/10.1039/c2jm16290c.

[9] M. Belaïche, M. Bakhache, M. Drillon, A. Derrory, S. Vilminot, Magnetic properties of MV2O6 compounds (M = Cu, Co, Ni), Phys. B Condens. Matter 305 (2001) 270–273, https://doi.org/10.1016/S0921-4526(01)00597-X.

[10] M. Lenertz, J. Alaria, D. Stoe, S. Colis, A. Dinia, D. Stoeffler, Magnetic Properties of Low-Dimensional r and γ CoV2O6, J. Phys. Chem. C 115 (2011) 17190–17196, https://doi.org/10.1021/jp2053772.

[11] Z. He, M. Itoh, Anisotropic magnetic behaviors of the spin-3/2 chain system γ-CoV2O6, J. Magn. Magn. Mater. 381 (2015) 263–266, https://doi.org/10.1016/j.jmmm.2015.01.007.

[12] S.A.J. Kimber, H. Mutka, T. Chatterji, T. Hofmann, P.F. Henry, H.N. Bordallo, D.N. Argyriou, J.P. Attfield, Metamagnetism and soliton excitations in the modulated ferromagnetic Ising chain CoV2O6, Phys. Rev. B 84 (2011) 104425, https://doi.org/10.1103/PhysRevB.84.104425.

[13] L. Dimesso, An alternate approach of the sol–gel method, preparation, properties, and applications, Handb. Sol-Gel Sci. Technol. Springer International Publishing, Cham, 2016, pp. 1–22, , https://doi.org/10.1007/978-3-319-19454-7_123-1.

[14] M.P. Pechini, 3.330.697, 1967.

[15] R.A. Young, The Rietveld Method, First, Oxford University Press, New York, 1993.

[16] H.M. Rietveld, A profile refinement method for nuclear and magnetic structures, J. Appl. Crystallogr. 2 (1969) 65–71, https://doi.org/10.1107/S0021889869006558.

[17] A.C. Larson, R.B. Von Dreele, Gen. Struct. Anal. Syst. (GSAS) (1994).

[18] B.H. Toby, EXPGUI, a graphical user interface for GSAS, J. Appl. Cryst. 34 (2001) 210–213.

[19] S. Seetharaman, H.L. Bhat, P.S. Narayanan, Raman spectroscopic studies on sodium metavanadate, J. Raman Spectrosc. 14 (1983) 401–405, https://doi.org/10.1002/jrs.1250140608.

[20] R. Tang, Y. Li, N. Li, D. Han, H. Li, Y. Zhao, C. Gao, P. Zhu, X. Wang, Reversible structural phase transition in ZnV_2O_6 at High Pressures, J. Phys. Chem. C 118 (2014) 10560–10566, https://doi.org/10.1021/jp411283m.

[21] R.L. Frost, K.L. Erickson, M.L. Weier, O. Carmody, Raman and infrared spectroscopy of selected vanadates, Spectrochim. Acta - Part A Mol. Biomol. Spectrosc. 61 (2005) 829–834, https://doi.org/10.1016/j.saa.2004.06.006.

[22] E.J. Baran, C.I. Cabello, Raman spectra of some MV_2O_6 metavanadates, J. Raman Spectrosc. 18 (1987) 405–407.

[23] Y. Li, R. Tang, N. Li, H. Li, X. Zhao, P. Zhu, X. Wang, Pressure-induced amorphization of metavanadate crystals SrV2O6 and BaV2O6, J. Appl. Phys. 118 (2015) 35902, https://doi.org/10.1063/1.4926784.

[24] M. Lenertz, A. Dinia, S. Colis, O. Mentré, G. André, F. Porcher, E. Suard, Magnetic structure of ground and field induced ordered states of low-dimensional γ-CoV2O6, J. Phys. Chem. C 118 (2014) 13981–13987, https://doi.org/10.1021/jp503389c.

[25] N. Hollmann, S. Agrestini, Z. Hu, Z. He, M. Schmidt, C.Y. Kuo, M. Rotter, A.A. Nugroho, V. Sessi, A. Tanaka, N.B. Brookes, L.H. Tjeng, Spectroscopic evidence for exceptionally high orbital moment induced by local distortions in α - CoV2 O6, Phys. Rev. B - Condens. Matter Mater. Phys. 89 (2014) 1–6, https://doi.org/10.1103/PhysRevB.89.201101.

[26] S.A.J. Kimber, D.N. Argyriou, J.P. Attfield, Metamagnetism and 1/3 Plateau in the Spin Chain Compound CoV_2O_6, Quantum. 8 (n.d.).

[27] M. Markkula, A.M. Arévalo-López, J.P. Attfield, Field-induced spin orders in monoclinic CoV2O6, Phys. Rev. B - Condens. Matter Mater. Phys. 86 (2012) 9–12, https://doi.org/10.1103/PhysRevB.86.134401.